

Cr(CO)<sub>4</sub>(PEt<sub>3</sub>). Even the more optimal conditions of providing Cr(CO)<sub>5</sub> access to a weaker S-H bond, i.e., that of PhSH, under photolytic conditions did not promote oxidative addition. Under the same conditions, however, oxidative chemistry is observed for the more readily oxidizable heavier metal cogener, (PhSH)W(CO)<sub>5</sub>. The latter results are consistent with earlier reports of the photolysis reaction of W(CO)<sub>6</sub> and PhSH or PhSSPh leading to (μ-PhS)<sub>2</sub>[W(CO)<sub>4</sub>]<sub>2</sub> and W(CO)<sub>2</sub>[(μ-PhS)<sub>2</sub>[W(CO)<sub>4</sub>]<sub>2</sub>]<sub>2</sub>.<sup>11</sup> Our results lend credence to a (PhSH)W(CO)<sub>5</sub> complex as intermediate in such reactions—and to the necessity of CO loss.

Oxidative addition of S-H is patently favored for d<sup>8</sup> Fe(0) complexes and the intermediate thiolate hydrides are stabilized by the presence of electron-donating ligands. For d<sup>6</sup> Cr(0) complexes, the RSH ligand loss path has a lower *E*<sub>act</sub>, and electron-donating ligands further lower this barrier for the Cr(CO)<sub>4</sub>L moiety—presumably due to an enhanced antibonding character of the S<sub>3p</sub>-Cr<sub>3d<sub>xy</sub></sub> HOMO. Clearly, for d<sup>6</sup> metals made extremely electron rich and possessing very labile ligands, such as Mo(diphos)<sub>2</sub>(N<sub>2</sub>)<sub>2</sub>, oxidative addition is expected and does readily occur.<sup>21</sup> A complete understanding of the contributing factors to

*E*<sub>act</sub>, such as open-site accessibility, metal oxidation potential, or possible structural rearrangements, awaits more detailed studies and theoretical analyses.

Finally we comment on the fact that solid-state Cr-S bond distances do not correlate with Cr-S bond lability in solution. The lower solution stability toward sulfur ligand loss of the RSH complexes as compared to the RS<sup>-</sup> derivatives is most reasonably due to the ability of the former to engage in hydrogen bonding, thus facilitating ligand loss via an interchange mechanism.

**Acknowledgment.** We acknowledge Drs. D. J. Darensbourg and P. J. Krusic for helpful discussion. The work was supported by the National Science Foundation (Grant CHE 86-03664). V.P. was an undergraduate fellow of the R. A. Welch Foundation.

**Supplementary Material Available:** Tables of crystallographic data, all bond lengths and bond angles, and anisotropic thermal parameters (3 pages); a listing of observed and calculated structure factors (5 pages). Ordering information is given on any current masthead page.

(21) Shortman, C.; Richards, R. L. *J. Organomet. Chem.* **1985**, *286*, C3.

Contribution from the Departments of Chemistry, University of Tennessee, Knoxville, Tennessee 37996-1600, and Duke University, Durham, North Carolina 27706

## Electrochemical Oxidative Addition Involving Dirhodium(I) Complexes Containing Transoid Bridging Bis(diphenylphosphino)methane Ligands. Crystal Structure of a Dirhodium(II) Complex with an Unusual Folding of the Diphosphine Ligand

Louis J. Tortorelli,<sup>†</sup> Clifton Woods,<sup>\*†</sup> and Andrew T. McPhail<sup>‡</sup>

Received April 11, 1989

The two-electron electrochemical oxidation of complexes such as [Rh<sub>2</sub>(μ-dppm)<sub>2</sub>(*t*-BuNC)<sub>2</sub>(μ-A)]PF<sub>6</sub> (dppm = bis(diphenylphosphino)methane; A = pyrazolate derivative) is facilitated by the presence of neutral Lewis bases such as pyridine derivatives or anionic ligands such as Cl<sup>-</sup>, Br<sup>-</sup>, I<sup>-</sup>, SCN<sup>-</sup>, NO<sub>3</sub><sup>-</sup>, and CH<sub>3</sub>COO<sup>-</sup>. Several of the oxidative-addition products have been isolated and characterized. The NO<sub>3</sub><sup>-</sup> and CH<sub>3</sub>COO<sup>-</sup> derivatives were also obtained by the reaction of the pyrazolato-bridged dirhodium(I) complexes with HNO<sub>3</sub> and CH<sub>3</sub>COOH, respectively. The paramagnetic Rh<sub>2</sub><sup>3+</sup> species generated by a one-electron oxidation of the parent dirhodium(I) complexes undergo disproportionation in the presence of the anionic ligands (except NO<sub>3</sub><sup>-</sup>). The addition of NO<sub>3</sub><sup>-</sup> to the Rh<sub>2</sub><sup>3+</sup> species results in oxidation to form a dinitrato Rh<sub>2</sub><sup>4+</sup> complex. The mechanism of the disproportionation reaction of the Rh<sub>2</sub><sup>3+</sup> species in the presence of halide ions is discussed. One mechanism is believed to involve electron exchange between two Rh<sub>2</sub><sup>3+</sup> species with simultaneous addition of two anions to the resulting Rh<sub>2</sub><sup>4+</sup> species. The operative mechanism depends on the nature of the Rh<sub>2</sub><sup>3+</sup> species and the nature of the anion. If the potential at which the anion ion is oxidized is more negative than the potential at which the Rh<sub>2</sub><sup>3+</sup> species is reduced, the mechanism involves the oxidation of the anion followed by an oxidative-addition reaction. This second mechanism was found to be operative for the reaction of some of the dicarbonyl Rh<sub>2</sub><sup>3+</sup> species with Br<sup>-</sup> and I<sup>-</sup>. The occurrence of different mechanisms for the disproportionation reactions is supported by the <sup>31</sup>P{<sup>1</sup>H} NMR data. When the electrochemical oxidation of the dirhodium(I) or the disproportionation of the dirhodium(I,II) complexes that contain the pyrazolate anion (pz) is conducted in CH<sub>2</sub>Cl<sub>2</sub> containing CH<sub>3</sub>COO<sup>-</sup> ions, the complex abstracts a Cl from the solvent to form [Rh<sub>2</sub>(μ-dppm)<sub>2</sub>(*t*-BuNC)<sub>2</sub>(μ-pz)Cl<sub>2</sub>]PF<sub>6</sub>, which was completely characterized by a single-crystal X-ray analysis. Crystals of the complex are monoclinic, space group *P*2<sub>1</sub>/*c*, with *a* = 12.355 (2) Å, *b* = 20.759 (9) Å, *c* = 24.689 (5) Å, β = 96.82 (2)°, *V* = 6287 (5) Å<sup>3</sup>, and *Z* = 4. The methylene moieties of the transoid bridging dppm ligands are folded away from the bridging pyrazolate ligand, and thus they have an orientation which contrasts with that previously found and believed to be favored for dppm-bridged A-frame complexes.

Transition-metal complexes containing diphosphine ligands have been the subjects of numerous investigations in recent years, in part because of their potential applications in homogeneous catalysis.<sup>1</sup> During catalytic processes, the metal centers invariably undergo oxidative-addition and reductive-elimination processes. Thus, factors affecting the propensities of metal centers to undergo these reactions are of considerable importance in designing more efficient catalytic agents. In this light, we have been investigating the effects of ligand modifications on the chemical and electrochemical oxidative processes involving diphosphine-bridged dirhodium complexes.

We recently reported some results of our investigations of pyrazolato-bridged dirhodium complexes that contain the Rh<sub>2</sub><sup>2+</sup> core and two transoid bridging bis(diphenylphosphino)methane

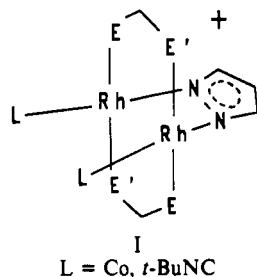
(dppm), (diphenylarsino)(diphenylphosphino)methane (dapm), or bis(diphenylarsino)methane (dpam) ligands.<sup>2</sup> These complexes were shown to have structure I. It was found that for the dicarbonyl complexes where there is no substituent (Y) in the 4-position of the pyrazolate ring, reactions with Cl<sub>2</sub> and Br<sub>2</sub> not only result in oxidative addition at the metal centers to produce complexes with the Rh<sub>2</sub><sup>4+</sup> core but also result in substitution at the 4-position of the heterocyclic ring. In contrast, the reaction with I<sub>2</sub> results only in oxidative addition at the metal centers.

Previous electrochemical studies of similar dirhodium complexes<sup>3</sup> indicate that coordinating species in solution drastically

<sup>†</sup> University of Tennessee.

<sup>‡</sup> Duke University.

- (1) Balch, A. L. In *Homogeneous Catalysis with Metal Phosphine Complexes*; Pignolet, L. H., Ed.; Plenum: New York, 1983; Chapter 5.
- (2) Sanger, A. R. In *Homogeneous Catalysis with Metal Phosphine Complexes*; Pignolet, L. H., Ed.; Plenum: New York, 1983; Chapter 6.
- (3) Puddephatt, R. J. *Chem. Soc. Rev.* **1983**, *12*, 99.
- (4) Janke, C. J.; Tortorelli, L. J.; Burn, J. L. E.; Tucker, C. A.; Woods, C. *Inorg. Chem.* **1986**, *25*, 4597.



affect the electrochemical behavior of the dinuclear species. This effect is ascribed to addition of the coordinating species to the metal centers during the oxidative process. The cyclic voltammograms of the complexes of structure I reveal that in a noncoordinating medium, if the potential sweep is in the positive direction, the complexes undergo two oxidative processes, a quasi-reversible electron transfer followed by an irreversible (or quasi-reversible in some cases) electron transfer.<sup>4</sup> The substitution of *tert*-butyl isocyanide for CO reduces the oxidation potential. The Rh<sub>2</sub><sup>2+</sup> diisocyanide complexes are therefore more susceptible to oxidation than their dicarbonyl analogues, and one-electron oxidations of the diisocyanide complexes produce stable and isolable paramagnetic Rh<sub>2</sub><sup>3+</sup> complexes.<sup>4</sup> A similar Rh<sub>2</sub><sup>3+</sup> complex that contains a bridging triazenido ligand has recently been prepared through chemical oxidation.<sup>5</sup>

Because of our continuing interest in the effects of ligand substitution and modification on the chemical, electrochemical, and structural properties of dppm-bridged dirhodium complexes, we describe herein the results of additional studies involving complexes of structure I. This report includes the structural characterization of a dirhodium complex that contains two transoid bridging dppm ligands and exhibits folding of the methylene groups of the dppm ligands away from the bridging apex ligand, an orientation previously believed to be unfavorable.

### Experimental Section

**Materials.** Procedures used for the syntheses of the dirhodium(I) pyrazolato-bridged complexes have been previously reported.<sup>2</sup> Pyrazole (Hpz), 4-methylpyrazole (H4mpz), and 3,5-dimethylpyrazole (H35mpz) were purchased from Aldrich Chemicals. 4-Bromo-3,5-dimethylpyrazole (H4B35mpz) was obtained from Pfaltz and Bauer, and 3,4,5-tribromopyrazole (H345Bpz) was prepared by a reported procedure.<sup>6</sup> Tetra-*n*-butylammonium halides were purchased from Aldrich and recrystallized three times from acetone/ether and dried in vacuo overnight at 70 °C. Tetra-*n*-butylammonium nitrate (TBAN), acetate (TBAA), and thiocyanate (TBASCN) were obtained from Fluka Chemicals. The TBAN was recrystallized from chloroform/ligroin and dried in vacuo overnight at 70 °C. TBAA and TBASCN were used as received. Tetra-*n*-butylammonium perchlorate (TBAP) was purchased from Eastman Kodak, recrystallized three times from water, and dried in vacuo overnight at 70 °C. Tetra-*n*-butylammonium hexafluorophosphate (TBAH) was prepared by the metathesis reaction of tetra-*n*-butylammonium iodide ((TBA)I) and KPF<sub>6</sub> in water, and it was purified by three recrystallizations from acetone-water followed by drying in vacuo overnight at 70 °C. Dichloromethane was dried over anhydrous CaCl<sub>2</sub> and freshly distilled under Ar from P<sub>2</sub>O<sub>5</sub> just prior to use.<sup>7</sup> Methanol was distilled and degassed with Ar immediately before use.

**Physical Measurements.** UV-vis spectra were recorded on a Cary 219 spectrophotometer in 1.0-cm quartz cells with degassed CH<sub>2</sub>Cl<sub>2</sub> as the solvent. Infrared (IR) spectra were recorded as Nujol mulls sealed between polyethylene sheets or as KBr pellets on either a Perkin-Elmer 1330 spectrophotometer or a Digilab FTS-20E Fourier transform spectrometer.

The electrochemical cell, equipment, and procedures used for doing cyclic voltammetry, coulometry, and controlled-potential electrolysis have

Table I. Compound Identification

1	[Rh <sub>2</sub> (μ-dppm) <sub>2</sub> (CO) <sub>2</sub> (μ-pz)]PF <sub>6</sub>
2	[Rh <sub>2</sub> (μ-dppm) <sub>2</sub> (CO) <sub>2</sub> (μ-35mpz)]PF <sub>6</sub>
3	[Rh <sub>2</sub> (μ-dppm) <sub>2</sub> (CO) <sub>2</sub> (μ-4mpz)]PF <sub>6</sub>
4	[Rh <sub>2</sub> (μ-dppm) <sub>2</sub> (CO) <sub>2</sub> (μ-4B35mpz)]PF <sub>6</sub>
5	[Rh <sub>2</sub> (μ-dppm) <sub>2</sub> (CO) <sub>2</sub> (μ-345Bpz)]PF <sub>6</sub>
6	[Rh <sub>2</sub> (μ-dppm) <sub>2</sub> ( <i>t</i> -BuNC) <sub>2</sub> (μ-pz)]PF <sub>6</sub>
7	[Rh <sub>2</sub> (μ-dppm) <sub>2</sub> ( <i>t</i> -BuNC) <sub>2</sub> (μ-35mpz)]PF <sub>6</sub>
8	[Rh <sub>2</sub> (μ-dppm) <sub>2</sub> ( <i>t</i> -BuNC) <sub>2</sub> (μ-4mpz)]PF <sub>6</sub>
9	[Rh <sub>2</sub> (μ-dppm) <sub>2</sub> ( <i>t</i> -BuNC) <sub>2</sub> (μ-4B35mpz)]PF <sub>6</sub>
10	[Rh <sub>2</sub> (μ-dppm) <sub>2</sub> ( <i>t</i> -BuNC) <sub>2</sub> (μ-345Bpz)]PF <sub>6</sub>
11	[Rh <sub>2</sub> (μ-dppm) <sub>2</sub> ( <i>t</i> -BuNC) <sub>2</sub> (μ-pz)]Cl <sub>2</sub> PF <sub>6</sub>

been reported elsewhere.<sup>4</sup> All electrochemical measurements were made by using the saturated calomel electrode (SCE) as the reference. Elemental analyses were performed by Galbraith Laboratories, Knoxville, TN. All <sup>31</sup>P{<sup>1</sup>H} NMR spectra were recorded on a JEOL FX 90Q Fourier transform spectrometer at 36.19 MHz with 85% H<sub>3</sub>PO<sub>4</sub> as the external reference.

**Preparation of [Rh<sub>2</sub>(μ-dppm)<sub>2</sub>(*t*-BuNC)<sub>2</sub>(μ-A)X<sub>2</sub>]PF<sub>6</sub> (A = pz, 4mpz, 35mpz, 4B35mpz, 345Bpz; X = Cl, Br, I, SCN). Method 1.** To prepare the chloride derivatives, chlorine gas<sup>2</sup> was bubbled through a stirred CH<sub>2</sub>Cl<sub>2</sub> solution of ca. 0.06 mmol of the appropriate parent dirhodium compound (Table I) at -77 °C. The resulting yellow solution was allowed to warm to room temperature and was stirred for 1.5 h. The volume was reduced to ca. 25 mL and a 1:1 mixture of ether/hexanes was added to precipitate a yellow-orange solid. The solid was collected by filtration and recrystallized from CH<sub>2</sub>Cl<sub>2</sub>/ether/hexanes to yield the desired products in 65–80% yield.

The bromides and iodides were prepared by slowly adding, via a transfer needle, 0.07 mmol of the halogen in 50 mL of CCl<sub>4</sub> to 150 mL of a stirred solution of 0.07 mmol of the appropriate parent dirhodium compound in CH<sub>2</sub>Cl<sub>2</sub> at -77 °C. The resulting solution was allowed to warm to room temperature, and the products were obtained in 80–90% yield by using the same procedure described above for the chlorides.

**Method 2.** The halide complexes and the SCN<sup>-</sup> analogues containing the pz, 4mpz, and 35mpz ligands were prepared electrochemically by oxidizing 50 mL of CH<sub>2</sub>Cl<sub>2</sub> solutions containing 0.1 M TBAH, ca. 0.07 mmol of the parent dirhodium complex, and at least a 3-fold molar quantity of the appropriate anion in the form of the tetra-*n*-butylammonium salt. The oxidations were performed at potentials that were 100–200 mV more positive than the peak potential of the irreversible two-electron oxidation wave exhibited by each solution. The volume of the oxidized solutions was reduced to ca. 10 mL after which 50 mL of CH<sub>3</sub>OH was added. The resulting solution was stirred overnight, during which time a precipitate formed. The crystalline solids were collected by filtration, recrystallized from CH<sub>2</sub>Cl<sub>2</sub>/ether/hexanes, and dried in vacuo. Anal. Calcd for [Rh<sub>2</sub>(μ-dppm)<sub>2</sub>(*t*-BuNC)<sub>2</sub>Cl<sub>2</sub>(μ-pz)]PF<sub>6</sub>·CH<sub>2</sub>Cl<sub>2</sub>, C<sub>64</sub>H<sub>67</sub>Cl<sub>4</sub>F<sub>6</sub>N<sub>4</sub>P<sub>3</sub>Rh<sub>2</sub>: C, 51.0; H, 4.5; Cl, 9.4. Found: C, 51.6; H, 4.6; Cl, 9.4. Anal. Calcd for [Rh<sub>2</sub>(μ-dppm)<sub>2</sub>(*t*-BuNC)<sub>2</sub>Br<sub>2</sub>(μ-pz)]PF<sub>6</sub>, C<sub>63</sub>H<sub>65</sub>Br<sub>2</sub>F<sub>6</sub>N<sub>4</sub>P<sub>3</sub>Rh<sub>2</sub>: N, 3.7; Br, 10.6. Found: N, 3.5; Br, 10.0.

**Preparation of [Rh<sub>2</sub>(μ-dppm)<sub>2</sub>(*t*-BuNC)<sub>2</sub>(μ-A)(NO<sub>3</sub>)<sub>2</sub>]PF<sub>6</sub> (A = pz, 4mpz, 35mpz, 4B35mpz, 345Bpz).** In a typical preparation, a THF solution containing 0.11 mL of 1.06 M HNO<sub>3</sub> (0.12 mmol) was added dropwise to a THF solution containing **8** (Table I) (78.6 mg, 0.06 mmol) and TBAH (55.1 mg, 0.14 mmol). After the mixture was stirred for ca. 2 h, the THF was removed via a rotary evaporator and the resulting residue was dissolved in CH<sub>2</sub>Cl<sub>2</sub>. Upon addition of a 1:1 mixture of ether/hexanes, an orange product appeared. The product was recrystallized from CH<sub>2</sub>Cl<sub>2</sub>/ether/hexanes. Yields were 85–95%. Anal. Calcd for [Rh<sub>2</sub>(μ-dppm)<sub>2</sub>(*t*-BuNC)<sub>2</sub>(μ-4mpz)(NO<sub>3</sub>)<sub>2</sub>]PF<sub>6</sub>·CH<sub>2</sub>Cl<sub>2</sub>, C<sub>65</sub>H<sub>69</sub>Cl<sub>2</sub>F<sub>6</sub>N<sub>6</sub>O<sub>6</sub>P<sub>3</sub>Rh<sub>2</sub>: C, 49.5; H, 4.4; N, 5.3. Found: C, 48.8; H, 5.1; N, 5.2.

**Preparation of [Rh<sub>2</sub>(μ-dppm)<sub>2</sub>(*t*-BuNC)<sub>2</sub>(μ-A)(CH<sub>3</sub>COO)<sub>2</sub>]PF<sub>6</sub> (A = pz, 4mpz, 35mpz, 4B35mpz, 345Bpz).** In a typical preparation, a THF solution of 0.29 mL of 1.81 M acetic acid (0.52 mmol) was added dropwise to a THF solution containing **6** (Table I) (73.1 mg, 0.05 mmol) and TBAH (43.5 mg, 0.11 mmol). After the mixture was stirred for 1 h, the THF was removed via a rotary evaporator and the resulting oil was dissolved in CH<sub>2</sub>Cl<sub>2</sub>. Upon the addition of a 1:1 mixture of ether/hexanes a golden-yellow product was obtained, which was recrystallized from CH<sub>2</sub>Cl<sub>2</sub>/ether/hexanes. Product yields were 75–80%. Anal. Calcd for [Rh<sub>2</sub>(μ-dppm)<sub>2</sub>(*t*-BuNC)<sub>2</sub>(μ-pz)(CH<sub>3</sub>COO)<sub>2</sub>]PF<sub>6</sub>·0.5CH<sub>2</sub>Cl<sub>2</sub>, C<sub>67.5</sub>H<sub>72</sub>Cl<sub>0.5</sub>F<sub>6</sub>N<sub>4</sub>O<sub>6</sub>P<sub>3</sub>Rh<sub>2</sub>: C, 53.6; H, 4.8; N, 3.7. Found: C, 53.6; H, 5.0; N, 3.7.

**X-ray Crystal Structure Analysis of [Rh<sub>2</sub>(μ-dppm)<sub>2</sub>(*t*-BuNC)<sub>2</sub>(μ-pz)-Cl<sub>2</sub>]PF<sub>6</sub>.** Preliminary unit cell parameters and space group information were obtained from oscillation and Weissenberg photographs. Intensity data for one quadrant of reciprocal space to θ = 67° were recorded on an Enraf-Nonius CAD-4 diffractometer (Cu Kα radiation, incident beam

- (a) Enlow, P. D.; Woods, C. *Inorg. Chem.* **1985**, *24*, 1273. (b) Womack, D. R.; Enlow, P. D.; Woods, C. *Inorg. Chem.* **1983**, *22*, 2653. (c) Woods, C.; Tortorelli, L. J. *Polyhedron* **1988**, *7*, 1751. (d) Tortorelli, L. J.; Tinsley, P. W.; Woods, C.; Janke, C. J. *Polyhedron* **1988**, *7*, 315.
- (4) Woods, C.; Tortorelli, L. J.; Rillema, D. P.; Burn, J. L. E.; DePriest, J. C. *Inorg. Chem.* **1989**, *28*, 1673.
- (5) Connelly, N. G.; Garcia, C. J. *Chem. Soc., Chem. Commun.* **1987**, 246.
- (6) *Chem. Abstr.* **1975**, *82*, 112068c.
- (7) Gordon, A. J.; Ford, R. A. *The Chemists Companion*; Wiley-Interscience: New York, 1972; p 434.

**Table II.** Spectroscopic Data for Complexes of the Type  $[\text{Rh}_2(\mu\text{-dppm})_2(t\text{-BuNC})_2(\text{ONO}_2)_2(\mu\text{-Z})](\text{PF}_6)^a$ 

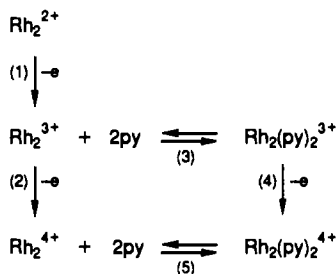
Z	IR <sup>b</sup>			<sup>31</sup> P NMR <sup>c</sup>		UV-vis <sup>d</sup> λ, nm (ε, M <sup>-1</sup> cm <sup>-1</sup> )
	ν(NC), cm <sup>-1</sup>	ν(NO <sub>2</sub> ), cm <sup>-1</sup>	ν(N—O), cm <sup>-1</sup>	δ, ppm	J, Hz	
pz	2182	1466, 1258	1003, 1007	16.2	92.8	480 (1500), 350 (17 200), 268 (29 000)
mpz	2180	1466, 1258	1000, 991	16.2	92.8	470 (2200), 350 (22 000), 266 (40 200)
35mpz	2178	1462, 1258	1001, 1011	14.3	92.8	480 (1400), 361 (26 000), 271 (38 000)
4B35mpz	2180	1462, 1258	1001	14.2	92.8	466 (700), 363 (13 000), 272 (19 000)
345Bpz	2180	1464, 1256	991	14.2	92.8	470 (1450), 366 (22 000), 278 (34 000)

<sup>a</sup>dppm = bis(diphenylphosphino)methane; pz = pyrazolate; 4mpz = 4-methylpyrazolate; 35mpz = 3,5-dimethylpyrazolate; 4B35mpz = 4-bromo-3,5-dimethylpyrazolate; 345Bpz = 3,4,5-tribromopyrazolate. <sup>b</sup>IR spectra obtained as KBr pellets. <sup>c</sup>NMR parameters were obtained from CH<sub>2</sub>Cl<sub>2</sub> solutions versus external H<sub>3</sub>PO<sub>4</sub> and are for AA'A''A'''XX' patterns with J = separation of the two major peaks. <sup>d</sup>UV-vis spectra obtained in CH<sub>2</sub>Cl<sub>2</sub>.

**Table III.** Spectroscopic Data for Complexes of the Type  $[\text{Rh}_2(\mu\text{-dppm})_2(t\text{-BuNC})_2(\text{OAc})_2(\mu\text{-Z})](\text{PF}_6)^a$ 

Z	IR <sup>b</sup>			<sup>31</sup> P NMR <sup>c</sup>		UV-vis <sup>d</sup> λ, nm (ε, M <sup>-1</sup> cm <sup>-1</sup> )
	ν(NC), cm <sup>-1</sup>	ν(C=O), cm <sup>-1</sup>	ν(C—O), cm <sup>-1</sup>	δ, ppm	J, Hz	
pz	2172	1601 (m), 1574 (w sh)	1358 (w sh), 1314 (m)	18.3	95.2	448 (5400), 385 (10 450), 312 (15 000), 253 (27 500)
mpz	2168	1599 (m), 1574 (w sh)	1358 (m), 1314 (m)	18.5	95.2	440 (4800), 386 (14 000), 315 (21 100), 248 (38 000)
35mpz	2168	1609 (m), 1599 (m)	1358 (m), 1314 (m)	16.2	95.2	470 (880), 376 (9050), 309 (12 200), 251 (18 000)
4B35mpz	2170	1603 (m)	1358 (m), 1314 (m)	16.1	95.2	180 (2300), 387 (28 000), 313 (39 000), 255 (60 000)
345Bpz				15.9	92.8	

<sup>a</sup>dppm = bis(diphenylphosphino)methane; pz = pyrazolate; 4mpz = 4-methylpyrazolate; 35mpz = 3,5-dimethylpyrazolate; 4B35mpz = 4-bromo-3,5-dimethylpyrazolate; 345Bpz = 3,4,5-tribromopyrazolate. <sup>b</sup>IR spectra obtained as KBr pellets. <sup>c</sup>NMR parameters were obtained from CH<sub>2</sub>Cl<sub>2</sub> solutions versus external H<sub>3</sub>PO<sub>4</sub> and are for AA'A''A'''XX' patterns with J = separation of the two major peaks. <sup>d</sup>UV-vis spectra obtained in CH<sub>2</sub>Cl<sub>2</sub>.

**Scheme I**

graphite monochromator, ω-2θ scans). From a total of 11 200 reflections, after equivalent forms were average, those 8067 reflections with  $I > 3.0\sigma(I)$  were retained for the structure analysis and corrected for the usual Lorentz and polarization effects. An empirical absorption correction, based on the φ dependence of the intensities of four reflections with χ ca. 90° ( $T_{\text{max}}:T_{\text{min}} = 1.0:0.69$ ), was also applied to these data. Refined unit cell parameters were derived by least-squares treatment of the CAD-4 diffractometer setting angles for 25 high-order reflections ( $57^\circ < \theta < 67^\circ$ ) widely separated in reciprocal space.

**Structure Analysis.** The crystal structure was solved by direct methods (MULTAN11/82). Approximate non-hydrogen atom positions were derived in part from an E map and from a series of difference Fourier syntheses. Full-matrix least-squares adjustment of positional and anisotropic temperature factor parameters, for these atoms, with hydrogen atoms included at their calculated positions in the later iterations, converged to  $R = 0.045$  ( $R_w = 0.059$ ).<sup>8,9</sup> For the structure-factor calculations, neutral-atom scattering factors and the real part of their anomalous dispersion corrections were taken from ref 10. In the least-squares iterations,  $\sum w\Delta^2$  [ $w = 1/\sigma^2(|F_o|)$ ;  $\Delta = (|F_o| - |F_c|)$ ] was minimized.

**Results**

The types of transformations observed in this work are summarized in Scheme I. Identification of the compounds is given in Table I, and spectroscopic data for the dinitrate and diacetate derivatives are given in Tables II and III, respectively. These data are discussed in the section that follows. A structure has been determined for  $[\text{Rh}_2(\mu\text{-dppm})_2(t\text{-BuNC})_2(\mu\text{-pz})\text{Cl}_2]\text{PF}_6$ , and is

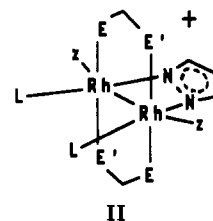
**Table IV.** Crystallographic Data for  $[\text{Rh}_2(\mu\text{-dppm})_2(t\text{-BuNC})_2\text{Cl}_2(\mu\text{-pz})]\text{PF}_6$  (11)

chem formula	C <sub>63</sub> H <sub>65</sub> Cl <sub>2</sub> F <sub>6</sub> N <sub>4</sub> P <sub>3</sub> Rh <sub>2</sub>	Z	4
fw	1423.81	$D(\text{calc})$ , g cm <sup>-3</sup>	1.645
space group	$P2_1/c$ (monoclinic, No. 14)	μ, cm <sup>-1</sup>	65.6
a, Å	12.355 (2)	radiation	Cu Kα, λ = 1.5418 Å
b, Å	20.759 (9)	temp, °C	22 (±1)
c, Å	24.689 (5)	$T_{\text{max}}:T_{\text{min}}$	1.00:0.61
β, deg	96.82 (2)	$R(R_w)$	0.045 (0.059)
V, Å <sup>3</sup>	6287 (5)		

presented below. Structural data are found in Tables IV–VII.

**Discussion**

**Chemical Oxidative Addition of Halogens.** Several of the diisocyanide complexes with structure I react with Cl<sub>2</sub>, Br<sub>2</sub>, and I<sub>2</sub> to give halide complexes with structure II. The products of the



halogen reactions exhibit values for ν(NC) that are about 50 cm<sup>-1</sup> higher than those of the parent compounds, a trend consistent with an increase in the oxidation state of the rhodium centers. The <sup>31</sup>P{<sup>1</sup>H} NMR data reveal that the halogenated products exhibit lower phosphorus chemical shifts than the parent complexes and are therefore consistent with a higher oxidation state of the Rh. These results led to the formulation of the halides as complexes containing the Rh<sub>2</sub><sup>4+</sup> core with a Rh–Rh bond.

The Rh<sub>2</sub><sup>2+</sup> diisocyanide complexes containing pyrazolate rings unsubstituted at the 4-position do not undergo substitution at that position during the reactions with Cl<sub>2</sub> and Br<sub>2</sub> as was observed for the dicarbonyl analogues.<sup>2</sup> The difference in reactivities of the dicarbonyl and diisocyanide complexes can probably be attributed to the different π-acceptor abilities of the two ligands. Carbon monoxide is a better π-acid than *t*-BuNC and appears to activate the 4-position of the pyrazolate ring.

(8) All crystallographic calculations were performed on a Microvax II computer by the use of the Enraf-Nonius Structure Determination Package.

(9)  $R = \sum ||F_o| - |F_c|| / \sum |F_o|$ ;  $R_w = \{ \sum w(|F_o| - |F_c|)^2 / \sum w|F_o|^2 \}^{1/2}$ .

(10) *International Tables for X-ray Crystallography*; Kynoch Press: Birmingham, England, 1974; Vol. IV.

**Table V.** Non-Hydrogen Atom Fractional Coordinates ( $\times 10^4$ ) and  $B_{eq}$  with Estimated Standard Deviations in Parentheses for  $[\text{Rh}_2(\mu\text{-dppm})_2(\mu\text{-pz})(t\text{-BuNC})_2\text{Cl}_2]\text{PF}_6$  (11)

atom	x	y	z	$B_{eq}, \text{\AA}^2$	atom	x	y	z	$B_{eq}, \text{\AA}^2$
Rh(1)	2863.5 (3)	2817.9 (2)	1705.5 (1)	2.308 (6)	C(211)	5779 (5)	1307 (3)	1830 (2)	3.6 (1)
Rh(2)	3063.2 (3)	1646.7 (2)	1190.9 (1)	2.300 (6)	C(212)	5562 (6)	666 (3)	1913 (3)	4.9 (1)
P(11)	4688.7 (11)	3108.7 (6)	1673.5 (5)	2.39 (2)	C(213)	6227 (6)	306 (4)	2301 (3)	6.0 (2)
P(12)	976.6 (11)	2764.9 (6)	1724.4 (5)	2.66 (2)	C(214)	7055 (7)	592 (4)	2615 (3)	7.3 (2)
P(21)	4994.7 (11)	1717.0 (6)	1259.9 (5)	2.43 (2)	C(215)	7275 (7)	1217 (5)	2544 (4)	7.8 (2)
P(22)	1131.8 (11)	1544.7 (6)	1021.9 (5)	2.63 (2)	C(216)	6658 (6)	1593 (4)	2133 (3)	5.6 (2)
Cl(1)	2876.3 (12)	3581.3 (6)	2483.5 (5)	3.58 (3)	C(211')	5679 (4)	1397 (2)	695 (2)	3.0 (1)
Cl(2)	3155.8 (12)	475.0 (6)	1026.8 (6)	3.88 (3)	C(212')	5628 (5)	749 (3)	573 (3)	4.8 (1)
P(5)	7508.6 (12)	1572.6 (9)	4602.2 (9)	5.43 (4)	C(213')	6208 (6)	493 (3)	179 (3)	5.3 (2)
F(1)	7635 (8)	2215 (3)	4312 (3)	15.7 (3)	C(214')	6893 (5)	877 (3)	-87 (3)	4.5 (1)
F(2)	7341 (7)	938 (3)	4875 (3)	15.7 (2)	C(215')	6959 (5)	1510 (3)	35 (3)	5.2 (1)
F(3)	7690 (10)	1904 (4)	5148 (3)	19.9 (4)	C(216')	6369 (5)	1780 (3)	423 (3)	4.9 (1)
F(4)	6412 (7)	1747 (6)	4646 (6)	25.2 (5)	C(221)	622 (4)	1373 (3)	310 (2)	3.2 (1)
F(5)	7265 (11)	1282 (4)	4073 (3)	23.8 (5)	C(222)	896 (7)	783 (3)	99 (3)	5.2 (2)
F(6)	8603 (6)	1455 (7)	4618 (6)	28.0 (6)	C(223)	453 (8)	612 (3)	-428 (3)	6.3 (2)
C(1)	5414 (4)	2551 (2)	1267 (2)	3.1 (1)	C(224)	-238 (6)	1019 (4)	-741 (3)	5.9 (2)
C(2)	383 (5)	2280 (3)	1144 (2)	3.3 (1)	C(225)	-500 (6)	1598 (4)	-537 (3)	5.0 (2)
C(111)	4823 (4)	3870 (2)	1327 (2)	2.9 (1)	C(226)	-74 (5)	1777 (3)	-11 (2)	4.2 (1)
C(112)	5497 (5)	3970 (3)	925 (2)	3.9 (1)	C(221')	401 (5)	922 (3)	1363 (2)	3.7 (1)
C(113)	5604 (5)	4574 (3)	699 (3)	4.5 (1)	C(222')	924 (5)	470 (3)	1705 (2)	4.1 (1)
C(114)	5043 (6)	5095 (3)	870 (3)	4.7 (1)	C(223')	320 (6)	17 (3)	1962 (3)	5.4 (2)
C(115)	4360 (6)	5010 (3)	1273 (3)	4.5 (1)	C(224')	-802 (6)	10 (4)	1865 (3)	6.0 (2)
C(116)	4247 (5)	4402 (3)	1495 (2)	3.8 (1)	C(225')	-1323 (5)	448 (4)	1512 (3)	5.5 (2)
C(111')	5545 (5)	3232 (3)	2322 (2)	3.5 (1)	C(226')	-739 (5)	909 (3)	1262 (3)	4.4 (1)
C(112')	5589 (6)	2754 (4)	2713 (3)	5.3 (2)	C(21)	3076 (4)	1845 (3)	424 (2)	3.0 (1)
C(113')	6183 (6)	2841 (5)	3221 (3)	7.1 (2)	N(22)	3148 (4)	1905 (3)	-35 (2)	3.8 (1)
C(114')	6727 (8)	3414 (5)	3332 (3)	8.5 (3)	C(23)	3300 (5)	1876 (4)	-618 (2)	4.6 (1)
C(115')	6688 (9)	3886 (5)	2956 (4)	9.9 (3)	C(24)	3670 (10)	1201 (5)	-730 (4)	10.2 (3)
C(116')	6101 (7)	3792 (4)	2437 (3)	7.4 (2)	C(25)	4195 (7)	2348 (5)	-711 (3)	8.4 (2)
C(121)	228 (5)	3523 (3)	1585 (2)	3.7 (1)	C(26)	2235 (7)	2043 (5)	-951 (3)	7.8 (2)
C(122)	-853 (6)	3519 (4)	1388 (4)	7.9 (2)	C(11)	2500 (4)	3322 (2)	1051 (2)	2.9 (1)
C(123)	-1428 (7)	4088 (4)	1279 (5)	9.5 (3)	N(12)	2234 (4)	3601 (2)	660 (2)	3.9 (1)
C(124)	-979 (7)	4654 (4)	1407 (4)	6.8 (2)	C(13)	1889 (6)	3968 (3)	163 (3)	5.2 (2)
C(125)	107 (7)	4680 (4)	1604 (4)	7.4 (2)	C(14)	1369 (10)	4578 (5)	335 (5)	11.8 (3)
C(126)	703 (6)	4113 (3)	1694 (4)	6.1 (2)	C(15)	1061 (9)	3560 (6)	-171 (4)	11.6 (3)
C(121')	464 (5)	2458 (3)	2337 (2)	2.6 (1)	C(16)	2887 (8)	4098 (5)	-104 (4)	9.8 (3)
C(122')	-138 (7)	2851 (4)	2643 (3)	6.8 (2)	N(1)	3157 (4)	2094 (2)	2280 (2)	3.04 (9)
C(123')	-500 (8)	2595 (5)	3118 (3)	8.2 (2)	N(2)	3177 (4)	1519 (2)	2026 (2)	2.94 (8)
C(124')	-236 (6)	2002 (5)	3297 (3)	6.5 (2)	C(3)	3354 (5)	1061 (3)	2410 (2)	3.7 (1)
C(125')	364 (6)	1615 (4)	2994 (3)	5.8 (2)	C(4)	3436 (6)	1349 (3)	2921 (2)	4.6 (1)
C(126')	709 (6)	1851 (3)	2516 (2)	4.6 (1)	C(5)	3296 (5)	2000 (3)	2817 (2)	3.8 (1)

$$^a B_{eq} = \frac{4}{3}[a^2\beta_{11} + b^2\beta_{22} + c^2\beta_{33} + ac(\cos\beta)\beta_{13}]$$

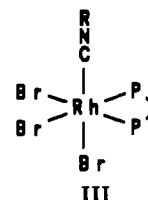
**Table VI.** Selected Bond Distances ( $\text{\AA}$ ) for  $[\text{Rh}_2(\mu\text{-dppm})_2(\mu\text{-pz})(t\text{-BuNC})_2\text{Cl}_2]\text{PF}_6$  (11)

Rh(1)-Rh(2)	2.768 (1)	Rh(1)-P(11)	2.345 (1)
Rh(1)-P(12)	2.340 (1)	Rh(1)-Cl(1)	2.489 (1)
Rh(1)-C(11)	1.933 (5)	Rh(1)-N(1)	2.069 (5)
Rh(2)-P(21)	2.377 (1)	Rh(2)-P(22)	2.383 (1)
Rh(2)-Cl(2)	2.471 (1)	Rh(2)-C(21)	1.940 (5)
Rh(2)-N(2)	2.067 (5)	C(21)-N(22)	1.154 (7)
N(22)-C(23)	1.475 (7)	C(11)-N(12)	1.140 (7)
N(12)-C(13)	1.464 (8)	N(1)-N(2)	1.350 (6)

**Table VII.** Selected Bond Angles (deg) for  $[\text{Rh}_2(\mu\text{-dppm})_2(\mu\text{-pz})(t\text{-BuNC})_2\text{Cl}_2]\text{PF}_6$  (11)

Rh(2)-Rh(1)-P(11)	94.14 (3)	P(22)-Rh(2)-C(21)	88.4 (1)
Rh(2)-Rh(1)-P(12)	96.38 (3)	P(22)-Rh(2)-N(2)	96.4 (1)
Rh(2)-Rh(1)-Cl(1)	157.05 (3)	Cl(2)-Rh(2)-C(21)	92.5 (2)
Rh(2)-Rh(1)-C(11)	96.7 (1)	Cl(2)-Rh(2)-N(2)	92.2 (1)
Rh(2)-Rh(1)-N(1)	70.0 (1)	C(21)-Rh(2)-N(2)	173.5 (2)
P(11)-Rh(1)-P(12)	167.75 (5)	P(11)-Rh(1)-Cl(1)	86.79 (5)
P(11)-Rh(1)-C(11)	87.8 (1)	P(11)-Rh(1)-N(1)	96.8 (1)
P(12)-Rh(1)-Cl(1)	85.96 (5)	P(12)-Rh(1)-C(11)	84.8 (2)
P(12)-Rh(1)-N(1)	92.6 (1)	Cl(1)-Rh(1)-C(11)	106.3 (1)
Cl(1)-Rh(1)-N(1)	87.1 (1)	C(11)-Rh(1)-N(1)	166.2 (2)
Rh(1)-Rh(2)-P(21)	93.25 (3)	Rh(1)-Rh(2)-P(22)	90.94 (3)
Rh(1)-Rh(2)-Cl(2)	161.52 (4)	Rh(1)-Rh(2)-C(21)	105.9 (2)
Rh(1)-Rh(2)-N(2)	69.8 (1)	P(21)-Rh(2)-P(22)	173.85 (4)
P(21)-Rh(2)-Cl(2)	90.38 (5)	P(21)-Rh(2)-C(21)	86.1 (1)
P(21)-Rh(2)-N(2)	89.3 (1)	P(22)-Rh(2)-Cl(2)	87.06 (5)
Rh(2)-C(21)-N(22)	172.8 (5)	Rh(1)-C(11)-N(12)	176.3 (4)
C(11)-N(12)-C(13)	179.1 (5)		

**Reaction of  $[\text{Rh}_2(\mu\text{-dppm})_2(t\text{-BuNC})_2(\mu\text{-4mpz})]\text{PF}_6$  (8) with Excess Bromine.** When 8 is treated with excess  $\text{Br}_2$ , the  $^3\text{1P}\{^1\text{H}\}$  NMR spectrum of the isolated product exhibits a simple doublet at 14.0 ppm with a  $J(\text{Rh-P})$  value of 78.1 Hz. This spectrum is in contrast to the non-first-order spectra with the typical AA'A''A'''XX' pattern observed for the symmetrical trans dppm-bridged dirhodium complexes. The NC stretching frequency of the *t*-BuNC ligands occurs at 2235  $\text{cm}^{-1}$ , a value which is about 60  $\text{cm}^{-1}$  higher than those observed for dimers containing Rh(II) centers and is consistent with values expected for a *t*-BuNC ligand coordinated to a Rh(III) center. This high  $\nu(\text{NC})$  results from the high oxidation state of Rh and the reduced  $\pi$  back-bonding between the Rh and the *t*-BuNC. The IR data reveal that there are no  $\text{PF}_6^-$  ions present, and the analytical data indicate that the Br:P:Rh ratio is 3:2:1. These data are consistent with the formulation of the product as the monomer  $\text{Rh}(\text{dppm})(t\text{-BuNC})\text{Br}_3$ . Since the  $^3\text{1P}\{^1\text{H}\}$  data indicate that the two phosphorus atoms are in equivalent environments, the complex is formulated as *fac*- $\text{Rh}(\text{dppm})(t\text{-BuNC})\text{Br}_3$ , shown as structure III. The deg-



radation of a  $\text{Rh}^{2+}$  dimer during oxidation to give mononuclear

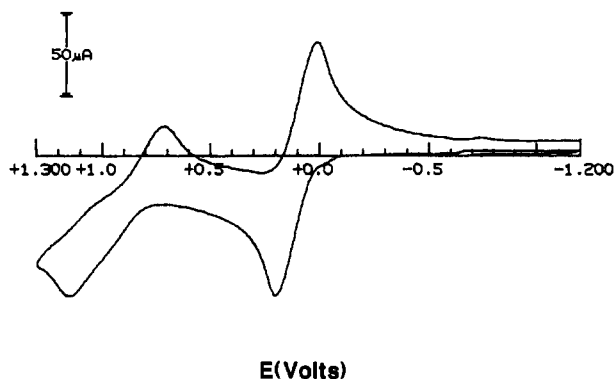


Figure 1. Cyclic voltammogram of **8** in  $\text{CH}_2\text{Cl}_2$  with 0.10 M TBAH.

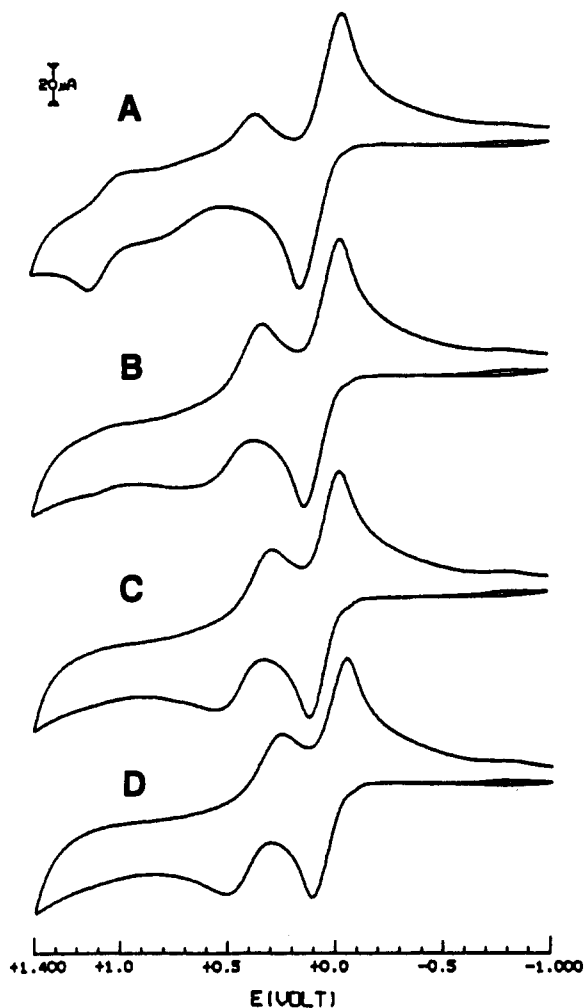


Figure 2. Cyclic voltammograms of a  $10^{-3}$  M  $\text{CH}_2\text{Cl}_2$  solution of **8** with 0.10 M TBAH and (A) 1.0, (B) 3.0, (C) 5.0, and (D) 10.0 equiv of pyridine.

rhodium(III) species has been reported.<sup>11</sup>

**Electrochemical Behavior.** The cyclic voltammogram shown in Figure 1 is typical of those observed for complexes **1–10** in the noncoordinating medium  $\text{CH}_2\text{Cl}_2/\text{TBAH}$ . For some dicarbonyl complexes both oxidation processes are quasi-reversible. Each oxidation wave corresponds to a one-electron oxidation process. It has been previously shown<sup>4</sup> for complexes **6–10** that controlled-potential electrolyses at potentials just past the first oxidation waves afford the isolable paramagnetic complexes  $[\text{Rh}_2(\mu\text{-dppm})_2(t\text{-BuNC})_2(\mu\text{-A})](\text{PF}_6)_2$  in which the unpaired electron

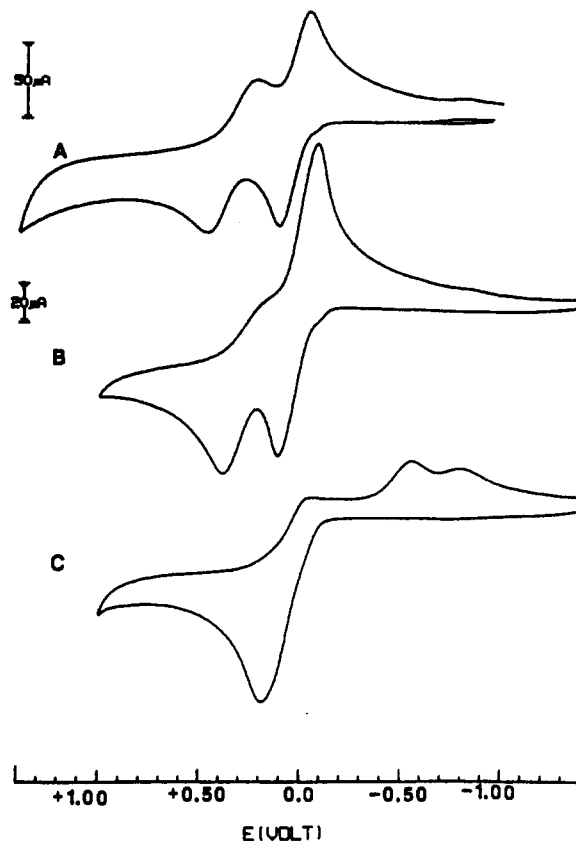


Figure 3. Cyclic voltammograms of  $10^{-4}$  M  $\text{CH}_2\text{Cl}_2$  solutions of **8** with 0.10 M TBAH and 20 equiv of (A) pyridine, (B) 3,5-dimethylpyridine, and (C) 4-(dimethylamino)pyridine.

is delocalized over the  $\text{Rh}_2^{3+}$  core. Complexes **1–5** can also be oxidized to form  $\text{Rh}_2^{3+}$  complexes. Although the paramagnetic dicarbonyl complexes are less stable than the corresponding diisocyanide complexes, they can be isolated and kept in an inert atmosphere for a couple of weeks. The  $\text{Rh}_2^{4+}$  complexes generated by oxidizing **1–10** in  $\text{CH}_2\text{Cl}_2/\text{TBAH}$  just past the second oxidation wave could not be isolated.

**Electrochemistry in the Presence of Neutral Coordinating Ligands.** The voltammograms shown in Figure 2 illustrate the effects on the electrochemical behavior of **8** resulting from addition of various equivalents of pyridine to the solution. With the addition of 1 equiv of pyridine, a new oxidation wave appears between the two original waves. Since pyridine is not oxidized at these potentials, this new wave indicates that a new species is formed. As the concentration of pyridine is increased, the peak current of the new wave increases and the peak potential decreases while the peak current of the original second oxidation wave decreases. After 10 equiv of pyridine have been added, the new wave appears as a second quasi-reversible wave with an  $E_{1/2}$  value closer to that of the first wave.

The effect that pyridine addition has on the electrochemical behavior of the diisocyanide complexes also depends on the basicity of the added pyridine. Shown in Figure 3 are the cyclic voltammograms of solutions containing 10 equiv of pyridine and the more basic 3,5-dimethylpyridine and 4-(dimethylamino)pyridine. It is clear from Figure 3 that as the basicity of the pyridine increases, the second oxidation wave, which appears during positive potential sweeps and results from the addition of the pyridine, moves closer to the first one-electron wave until the two waves coalesce into a single two-electron wave for the most basic pyridine, 4-(dimethylamino)pyridine. These data indicate that coordinating species such as pyridine facilitate removal of the second electron to the point that for strongly coordinating species the oxidation becomes a two-electron electrochemically irreversible process.

The effects of the pyridine addition on the electrochemical behavior of the dirhodium diisocyanide complexes can be explained by using Scheme I. Dominant electron-transfer processes in the

(11) Blach, A. L.; Labadie, J. W.; Delker, G. *Inorg. Chem.* **1979**, *18*, 1224.

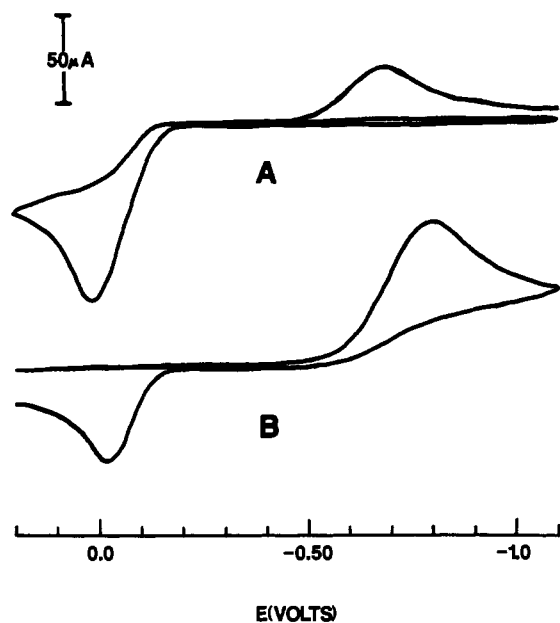


Figure 4. Cyclic voltammograms of **8** in  $\text{CH}_2\text{Cl}_2$  with 0.10 M TBAH, and  $\text{Br}^-$  added (A) before oxidation or (B) after oxidation.

presence of weakly basic pyridines or low concentrations of the pyridines are steps 1 and 2, and the oxidation waves of the parent dirhodium species are the main features. When bulk electrolysis is performed past the second oxidation wave of the parent species and excess pyridines are added to the oxidized solution, step 5 of Scheme I occurs. As the concentration or the basicity of the pyridine increases, the equilibrium step (3) shifts to the right, increasing the concentration of the diadduct, which gives rise to an oxidation wave with a peak potential lying between those of the original one-electron waves. Thus, the peak current for the wave associated with step 2 decreases and that of the new wave, which is associated with step 4, increases with increasing formation of the diadduct  $\text{Rh}_2(\text{py})_2^{3+}$ . In the presence of strongly basic pyridines, the oxidation step (4) becomes as favorable as step 1 and results in a two-electron oxidation that produces the dirhodium (II) diadduct.

**Electrochemical Oxidative Addition of Anionic Ligands to  $[\text{Rh}_2(\mu\text{-dppm})_2(t\text{-BuNC})_2(\mu\text{-A})]\text{PF}_6$  (A = Pyrazolate Derivative).** The cyclic voltammogram shown in Figure 4 is typical of those obtained for the pyrazolato-bridged dirhodium complexes in  $\text{CH}_2\text{Cl}_2/\text{TBAH}/\text{X}^-$  ( $\text{X}^- = \text{Cl}^-$ ,  $\text{Br}^-$ , and  $\text{I}^-$ ). The oxidation wave near +0.05 V is a two-electron wave and indicates that the effect of halide ions on the electrochemical behavior of the dirhodium(I) complexes is similar to that of the pyridine derivatives in that they facilitate removal of the second electron from the  $\text{Rh}_2^{2+}$  species to produce a  $\text{Rh}_2^{4+}$  species with structure II. Rh(I) is a  $d^8$  metal center and prefers a square-planar environment; however, Rh(II) is a  $d^7$  center and prefers a higher coordination number. Thus, the Rh(II) is stabilized by the coordination of the halide ion during electrochemical oxidation. In contrast to some of the dicarbonyl complexes, the halide complexes obtained via electrochemical oxidative addition of the diisocyanide complexes are identical with those obtained by chemical oxidation with halogens.

Complexes **6–10** in the medium  $\text{CH}_2\text{Cl}_2/\text{TBAH}/\text{SCN}^-$  exhibit the same cyclic voltammetric behavior as that shown in Figure 4; however, unlike the halide derivatives, all of the  $\text{SCN}^-$  derivatives do not exhibit  $^{31}\text{P}\{\text{H}\}$  NMR spectra consisting of a single well-defined AA'A''A'''XX' pattern that would be expected for a single symmetrical species of structure II. All attempts to generate complexes that give a symmetrical NMR pattern resulted in species whose  $^{31}\text{P}\{\text{H}\}$  NMR spectra consist of overlapping multiplets (Figure S1). It is possible that, due to the ambidentate nature of  $\text{SCN}^-$ , the oxidation product is a mixture of isomers with S-bound and N-bound  $\text{SCN}^-$  ligands, since NC stretching frequencies are observed in the regions where stretching frequencies for N-bound and S-bound  $\text{SCN}^-$  ligands are expected.<sup>12</sup>

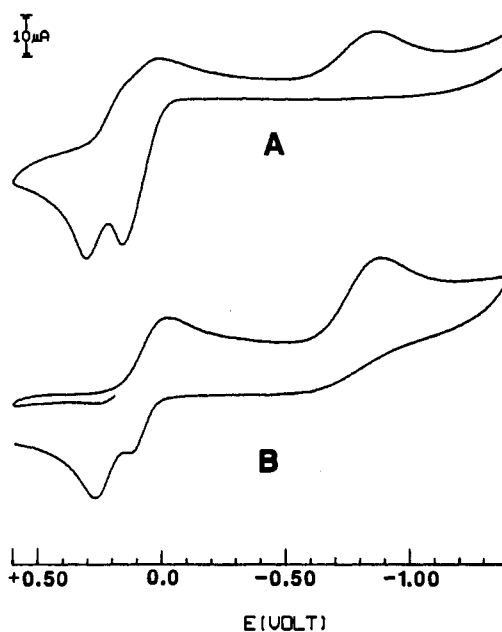


Figure 5. Cyclic voltammograms of  $10^{-3}$  M  $\text{CH}_2\text{Cl}_2$  solutions of **8** with 0.10 M TBAN (A) before oxidation at 0.40 V or (B) after oxidation at 0.40 V vs SCE.

It was desirable to investigate the electrochemical oxidative-addition of other anions with several potential bonding modes. The ions chosen were  $\text{ClO}_4^-$ ,  $\text{NO}_3^-$ , and  $\text{CH}_3\text{COO}^-$ . If these ions were to coordinate, they could do so as terminal monodentate ligands, chelating ligands, or bidentate bridging ligands. Though the  $\text{ClO}_4^-$  is generally considered to be a poor coordinating ligand, we have observed<sup>13</sup> that when compared with  $\text{PF}_6^-$ , it can sometimes have a noticeable effect on the cyclic voltammetric behavior of dirhodium complexes, presumably by weakly coordinating to the metal center or through ion pairing. The cyclic voltammetric behavior of the pyrazolato-bridged dirhodium complexes in the presence of  $\text{ClO}_4^-$  exhibits few observable differences from that observed in the presence of  $\text{PF}_6^-$ . These observations suggest that the effect of  $\text{ClO}_4^-$  is negligible; however, a two-electron oxidation of the species in the presence of  $\text{ClO}_4^-$  generates several phosphorus-containing species as evidenced by the  $^{31}\text{P}\{\text{H}\}$  NMR spectra of the oxidized solution. This behavior is in contrast with that observed in the presence of  $\text{PF}_6^-$  where a species that exhibits only a AA'A''A'''XX' pattern is generated, though the species cannot be isolated.

The  $\text{NO}_3^-$  ion is generally accepted as being a better coordinating ligand than  $\text{ClO}_4^-$ , and indeed we have previously generated and structurally characterized a dirhodium complex with a bridging nitrate ligand.<sup>14</sup> The effect of nitrate on the cyclic voltammetric behavior of the diisocyanide complexes can be seen by comparing the voltammogram of  $[\text{Rh}_2(\mu\text{-dppm})_2(t\text{-BuNC})_2(\mu\text{-pz})]\text{PF}_6$  in  $\text{CH}_2\text{Cl}_2/\text{TBAH}$  in Figure 1 with that of  $[\text{Rh}_2(\mu\text{-dppm})_2(t\text{-BuNC})_2(\mu\text{-4B35mpz})]\text{PF}_6$  in  $\text{CH}_2\text{Cl}_2/\text{TBAN}$  in Figure 5A. The effect of nitrate is similar to that of the halides in that the quasi-reversible electron transfer becomes more irreversible and in the sense that the nitrate ion facilitates the removal of the second electron. However, the removal of the second electron is not facilitated by nitrate to the extent that a single two-electron oxidation wave is observed as in the case of the halides, but instead two irreversible one-electron waves are observed.

The cyclic voltammetric behavior of  $[\text{Rh}_2(\mu\text{-dppm})_2(t\text{-BuNC})_2(\mu\text{-4B35mpz})]\text{PF}_6$  after controlled-potential electrolysis

- (12) (a) Nakamoto, K. *Infrared and Raman Spectra of Inorganic Coordination Compounds*; Wiley-Interscience: New York, 1978. (b) Bailey, R. A.; Kozak, S. L.; Michelsen, T. W.; Mills, W. N. *Coord. Chem. Rev.* **1971**, *6*, 407.  
 (13) Tortorelli, L. J.; Woods, C. Unpublished results.  
 (14) Tortorelli, L. J.; Tucker, C. A.; Woods, C.; Bordner, J. *Inorg. Chem.* **1986**, *25*, 3534.

at potentials more positive than the second wave in  $\text{CH}_2\text{Cl}_2/\text{TBAN}$  is shown in Figure 5B and illustrates that the process is chemically reversible. All of the nitrate products are orange solids whose spectroscopic data are given in Table II. The  $^{31}\text{P}\{^1\text{H}\}$  NMR spectra of the oxidized solutions exhibit the symmetrical AA'A''A'''XX' pattern. Problems were encountered in separating the oxidation products from the supporting electrolyte; therefore, the nitrate products were not isolated from the electrolysis solution. When the parent dirhodium complexes were treated with  $\text{HNO}_3$ , the products analyzed as dinitrates and gave  $^{31}\text{P}\{^1\text{H}\}$  NMR spectra identical with those of the electrochemically-generated products. It was concluded that the two products were the same.

The NMR chemical shifts and IR data in Table II are consistent with the presence of a  $\text{Rh}_2^{4+}$  core. All nitrate complexes exhibit IR bands that, on the basis of previous work,<sup>12,15</sup> have been assigned to the antisymmetric  $\text{NO}_2$ , symmetric  $\text{NO}_2$ , and  $\text{NO}$  stretching vibrations of a terminal monodentate nitrate ligand. These results, coupled with analytical data, led to the conclusion that the nitrate complexes have structure II ( $Z = \text{ONO}_2$ ). Attempts to grow crystals suitable for X-ray analysis were unsuccessful.

When tetra-*n*-butylammonium acetate (TBAA) was used as a source of acetate ions, the cyclic voltammogram of **6** in  $\text{CH}_2\text{Cl}_2/\text{TBAH}/\text{TBAA}$  was analogous to that shown in Figure 4 with the anodic wave at +0.018 V and the cathodic wave at -1.08 V. Controlled-potential coulometry at +0.150 V indicated that the oxidation was a two-electron process. The  $^{31}\text{P}\{^1\text{H}\}$  NMR spectrum of the oxidation product reveals the AA'A''A'''XX' pattern with a chemical shift of 3.91 ppm and a  $[^1J(\text{Rh}-\text{P}) + ^2J(\text{Rh}-\text{P})]$  value of 92.8 Hz. The IR spectrum of the product indicates the presence of terminal isocyanide ligands and  $\text{PF}_6^-$  ions. A crystal structure analysis (vide infra) revealed that the oxidation product is the chloride-containing species  $[\text{Rh}_2(\mu\text{-dppm})_2(t\text{-BuNC})_2\text{Cl}_2(\mu\text{-pz})]\text{PF}_6$  (**11**). Since **11** was an unexpected product, the results of the oxidation were verified by repeating the experiment several times; thus, it was concluded that the solvent,  $\text{CH}_2\text{Cl}_2$ , was the source of  $\text{Cl}^-$ . In order to verify this conclusion, the oxidation was performed in acetone. An oxidation product could not be separated from the supporting electrolyte used in the acetone medium; therefore, tetra-*n*-butylammonium tetrafluoroborate (TBAF) was used as the supporting electrolyte and the oxidation was monitored with  $^{31}\text{P}\{^1\text{H}\}$  NMR spectroscopy. The  $^{31}\text{P}\{^1\text{H}\}$  NMR spectrum of the oxidation product taken in  $(\text{CH}_3)_2\text{CO}/\text{TBAF}/\text{TBAA}$  reveals a AA'A''A'''XX' pattern with a chemical shift of 18.4 ppm and a  $[^1J(\text{Rh}-\text{P}) + ^2J(\text{Rh}-\text{P})]$  value of 95.2 Hz. It is clear that the oxidation products obtained in the two media are different. The NMR data of the product obtained in the acetone medium are identical with those of a product obtained by reacting **6** with acetic acid;<sup>13</sup> thus, the acetate derivatives whose spectroscopic data are found in Table III were prepared via the acetic acid reactions. The product obtained with **6** gave analytical data that are consistent with the formula  $[\text{Rh}_2(\mu\text{-dppm})_2(t\text{-BuNC})_2(\text{OOCCH}_3)_2(\mu\text{-pz})]\text{PF}_6$ ; thus, the acetate derivatives were assigned structure II.

Since a two-electron electrochemical oxidation of **6** in  $\text{CH}_2\text{Cl}_2/\text{TBAH}$  does not produce the dichloride oxidative-addition product in the absence of acetate ions, it is clear that the acetate ion facilitates the abstraction of chloride from the solvent by the dirhodium species during the oxidation. The mechanism of this process is not known, nor is the fate of the acetate ion known at this time.

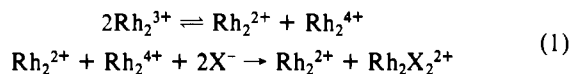
**Disproportionation of  $[\text{Rh}_2(\mu\text{-dppm})_2(\mu\text{-A})\text{L}_2]\text{PF}_6$  (A = Pyrazolate Derivative; L = CO, *t*-BuNC) in the Presence of Anionic Ligands.** In the presence of certain anionic ligands, the one-electron oxidized species containing the  $\text{Rh}_2^{3+}$  core undergo disproportionation to give the parent  $\text{Rh}_2^{2+}$  species and a  $\text{Rh}_2^{4+}$  species of structure II. A similar disproportionation reaction involving chloride and an analogous dirhodium species has been previously observed.<sup>16</sup>

When halide ions are added to solutions of the diisocyanide  $\text{Rh}_2^{3+}$  complexes, the resulting solutions exhibit  $^{31}\text{P}\{^1\text{H}\}$  NMR spectra that contain two AA'A''A'''XX' patterns. One signal is identical with that of the  $\text{Rh}_2^{2+}$  parent compound and the other is that of the corresponding dihalide of structure II. When  $\text{SCN}^-$  is added to solutions of **6**<sup>+</sup>, **7**<sup>+</sup>, and **8**<sup>+</sup>, the NMR spectra contain the symmetrical patterns of the parent compounds and more complex multiplets identical with those observed for the electrochemically generated thiocyanate product. The addition of acetate ions to a  $\text{CH}_2\text{Cl}_2$  solution containing **6**<sup>+</sup> produces **6** and the dichloride of structure II. In acetone, the disproportionation reaction gives the parent compound and the expected diacetate derivatives.

No reaction occurs upon the addition of  $\text{ClO}_4^-$  to the diisocyanide  $\text{Rh}_2^{3+}$  species. When  $\text{NO}_3^-$  is added to **6**<sup>+</sup>, disproportionation does not occur; instead, a reaction to produce a single product is observed. The  $^{31}\text{P}$  NMR data are identical with those of the nitrate product of structure II that was generated via electrochemical oxidation of **6** in the presence of TBAN (Table II). Thus, the addition of nitrate to solutions containing  $\text{Rh}_2^{3+}$  species results only in oxidation of the dirhodium complex. The reduction product was not identified.

The  $\text{Rh}_2^{3+}$  species formed from the dicarbonyl species **1** and **4** have been shown to undergo disproportionation in the presence of  $\text{Cl}^-$ . For the products containing 4B35mpz, the  $^{31}\text{P}\{^1\text{H}\}$  NMR chemical shifts and coupling constants are identical with those of the parent compound **4** and its dichloride of structure II. The disproportionation products obtained from the dicarbonyl species that contains pz exhibit a  $^{31}\text{P}\{^1\text{H}\}$  NMR resonance identical with that of **1**; however, the  $\text{Rh}_2^{4+}$  dichloride species produced has a chemical shift of 11.35 ppm whereas the dichloride obtained by treating **1** with  $\text{Cl}_2$  has a chemical shift of 10.68 ppm. This difference is attributed to the fact that reaction of **1** with  $\text{Cl}_2$  leads to substitution in the 4-position of the pyrazolate ring whereas the disproportionation reaction does not result in substitution at this position. The lower chemical shift of the 4-chloropyrazolate species is consistent with the observation of a lower chemical shift for the 4B35mpz complex than for the 35mpz complex.

We have previously shown<sup>4</sup> that when solutions of the  $\text{Rh}_2^{2+}$  species and the electrochemically generated  $\text{Rh}_2^{4+}$  species are mixed, a comproportionation reaction occurs to produce the  $\text{Rh}_2^{3+}$  species. It is likely that, in solutions that contain the  $\text{Rh}_2^{3+}$  species, an electron exchange between two  $\text{Rh}_2^{3+}$  species occurs to establish an equilibrium involving small quantities of the  $\text{Rh}_2^{2+}$  and  $\text{Rh}_2^{4+}$  species. The cyclic voltammetric data presented earlier clearly indicate that coordination of halide ions greatly stabilizes the  $\text{Rh}_2^{4+}$  core by forming species of structure II. Therefore, when halide ions are added to solutions containing  $\text{Rh}_2^{3+}$  species, the stability of the  $\text{Rh}_2^{4+}$  species is greatly enhanced and the equilibrium is driven sharply to the right via the mechanism shown in eq 1.



When the potential at which the halide ion is oxidized is approximately equal to or less than the potential at which the  $\text{Rh}_2^{3+}$  is reduced, another mechanism for the generation of the products shown in eq 1 is possible. This situation arises for the dicarbonyl  $\text{Rh}_2^{3+}$  species **1**<sup>+</sup> and  $\text{Br}^-$  and  $\text{I}^-$ . The  $\text{Rh}_2^{3+}$  species oxidizes the halide ion, generating a halogenating agent and the corresponding  $\text{Rh}_2^{2+}$  species. The halogenating agent subsequently reacts with some of the  $\text{Rh}_2^{2+}$  species to produce the disproportionation products  $\text{Rh}_2^{2+}$  and  $\text{Rh}_2\text{X}_2^{2+}$ . Support for this mechanism is obtained from an NMR analysis of the products of the disproportionation reaction of  $\text{Br}^-$  with the dicarbonyl species **1**<sup>+</sup>. The  $\text{Rh}_2^{4+}$  species generated in the reaction has identical NMR data as  $[\text{Rh}_2(\mu\text{-dppm})_2(\text{CO})_2(\mu\text{-4Bpz})\text{Br}_2]\text{PF}_6$  (4Bpz = 4-bromopyrazolate). Since this complex contains a bromo substituent on the pyrazolate ring, it is clear that a species capable of brominating

(15) (a) Rosenthal, M. R. *J. Chem. Educ.* **1973**, *50*, 331. (b) Addison, C. C.; Gatehouse, B. M. *J. Chem. Soc.* **1960**, 613.

(16) Boyd, D. C.; Matsch, P. A.; Mixa, M. M.; Mann, K. R. *Inorg. Chem.* **1986**, *25*, 3333.

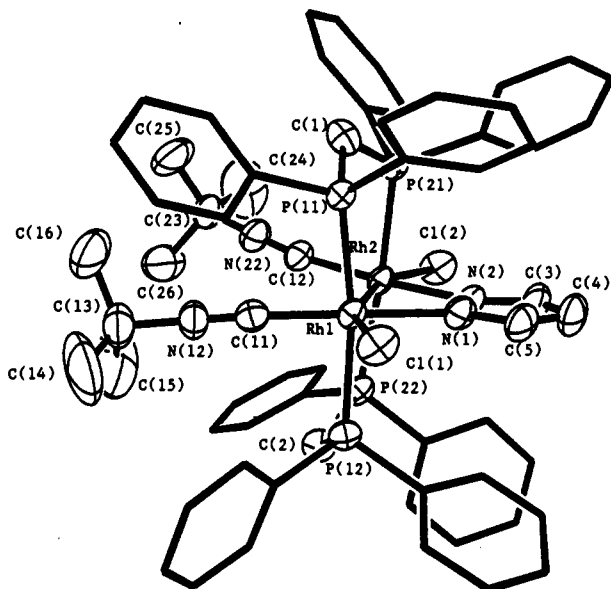


Figure 6. Partial ORTEP projection of  $[\text{Rh}_2(\mu\text{-dppm})_2(t\text{-BuNC})_2(\mu\text{-pz})\text{Cl}_2]^+$  with thermal ellipsoids at 50% probability.

the pyrazolate ring is generated during the reaction of the  $\text{Rh}_2^{3+}$  species with  $\text{Br}^-$ . Though some contribution from a mechanism such as that outlined in eq 1 cannot be ruled out, it is clear that another mechanism plays a role in generating the products of the reaction of the dicarbonyl derivatives with  $\text{Br}^-$  since halogenation of the pyrazolate ring does not occur for the diisocyanide derivatives.

A  $^{31}\text{P}$  NMR analysis of the reaction of the dicarbonyl  $\text{Rh}^{3+}$  species with  $\text{Br}^-$  indicates that the NMR signal of the  $\text{Rh}_2^{4+}$  species is less intense than that of the  $\text{Rh}_2^{2+}$  species. Since 1 equiv of  $\text{Br}^-$  was used per  $\text{Rh}_2^{3+}$  unit, the stoichiometry of the reaction does not allow for the formation of equal amounts of the  $\text{Rh}_2^{2+}$  and  $\text{Rh}_2^{4+}$  species when the pyrazolate ring is brominated. In those cases where ring substitution does not occur, the  $^{31}\text{P}$  NMR intensity data suggest that approximately equal amounts of the two products are obtained.

Since  $\text{I}^-$  is oxidized at less positive potentials than  $\text{Br}^-$ , it is possible that the disproportionation of the dicarbonyl  $\text{Rh}_2^{3+}$  species in the presence of  $\text{I}^-$  occurs via a mechanism that initially involves the oxidation of  $\text{I}^-$ . Iodination of the pyrazolate ring at the 4-position was not expected to occur, and the generation of equal amounts of the  $\text{Rh}_2^{2+}$  and  $\text{Rh}_2^{4+}$  species was experimentally verified by  $^{31}\text{P}$  NMR spectroscopy.

**X-ray Structure Analysis of  $[\text{Rh}_2(\mu\text{-dppm})_2(t\text{-BuNC})_2\text{Cl}_2(\mu\text{-pz})]\text{PF}_6$  (11).** An ORTEP drawing of 11 is presented in Figure 6. Crystal data are provided in Table IV, non-hydrogen atom coordinates are in Table V, and selected bond lengths and bond angles are in Tables VI and VII, respectively.

The solid-state structure consists of cationic binuclear rhodium(II) species and  $\text{PF}_6^-$  ions in a 1:1 ratio with four formula units occupying the general positions of the space group  $P2_1/c$ . Each Rh atom is six-coordinate, with the inner coordination sphere, a distorted octahedron, consisting of two P atoms, a N atom (from the pyrazolate), a Cl atom, a C atom (from the *t*-BuNC), and a second Rh atom. Structural data have been reported for the analogous complex  $[\text{Rh}_2(\mu\text{-dppm})_2(\text{CO})_2\text{I}_2(\mu\text{-35mpz})]\text{PF}_6$  (12)<sup>17</sup> and the related complexes  $[\text{Rh}_2(\mu\text{-dppm})_2(\text{CO})_2(\mu\text{-35mpz})]\text{PF}_6$  (13)<sup>17</sup> and  $[\text{Rh}_2(\mu\text{-dpam})_2(\text{CO})_2(\mu\text{-35mpz})]\text{PF}_6$  (14).<sup>2</sup> In the case

of 11, one noticeable distortion from an octahedral environment is the Rh–Rh–Cl angle of  $157.05(3)^\circ$  for one central Rh atom and  $161.52(4)^\circ$  for the other. For complex 12, the analogous Rh–Rh–I angles are  $174.6(1)^\circ$ . The larger deviation of the halide from the Rh–Rh vector for 11 than for 12 is probably due, in part, to the fact that in 11 the chloride is cis to a *t*-BuNC ligand whereas in 12 the iodide is cis to the less sterically demanding CO. The Rh–Rh distance of  $2.768(1) \text{ \AA}$  compares favorably with those of other complexes with a Rh–Rh single bond.<sup>18</sup> The Rh–P distances are also within the range of  $2.303\text{--}2.367 \text{ \AA}$  found for some other *trans* dppm-bridged dirhodium complexes.<sup>17,19</sup>

The Rh–C (from CO) bond distances of  $1.80(2) \text{ \AA}$  found in 12 are much shorter than the Rh–C (from *t*-BuNC) bond distances of  $1.933(5)$  and  $1.940(5) \text{ \AA}$  observed for 11, probably owing in part to the better  $\pi$ -accepting ability of CO compared to RNC.

The most significant structural feature of 11 is the orientation of the methylene moieties of the dppm ligands. In most previously determined structures of *trans* dppm-bridged dirhodium A-frame and related complexes, the methylene groups are always folded over the bridging ligand in the apex position. It has been argued that this orientation allows the bulky phenyl groups on the side with the apex ligand to occupy more open sites, thus minimizing unfavorable intramolecular contacts. The dihedral angle between the Rh(1)–Rh(2)–P(11)–P(12) and Rh(2)–Rh(1)–P(21)–P(22) least-squares planes is  $10.2^\circ$ , and thus the  $\text{Rh}_2\text{P}_4$  core is not planar. Each of the Rh–Rh–P–C–P rings in 11 is in a half-chair conformation. It is apparent from Figure 6 that the pyrazolate ligand and the methylene moieties lie on opposite sides of the least squares plane through the  $\text{Rh}_2\text{P}_4$  core ( $\Delta\text{N}(1) = -2.02$ ;  $\Delta\text{N}(2) = -2.01$ ;  $\Delta\text{C}(1) = 0.60$ ;  $\Delta\text{C}(2) = 0.66 \text{ \AA}$ ). This orientation of the methylene groups in 11 must be related to the steric demands of the *t*-BuNC ligands; however, the size of the *t*-BuNC group cannot be the only factor since we have recently determined the structure of the related dirhodium complex  $[\text{Rh}_2(\mu\text{-dppm})_2(t\text{-BuNC})_2(\mu\text{-35mpz})]\text{PF}_6$ <sup>13</sup> that also contains *t*-BuNC ligands *trans* to a pyrazolate derivative, and the methylene groups are folded over the bridging pyrazolate ligand as expected. After this work was submitted for publication, the structure of the analogous diiodide complex was reported.<sup>20</sup>

**Acknowledgment.** We thank the National Science Foundation and Research Corp. for funds for partial support of this work and Johnson Matthey, Inc., for a generous loan of rhodium trichloride. We also thank Professor James Q. Chambers of the Department of Chemistry of the University of Tennessee for some helpful comments concerning the electrochemistry. C.W. wishes to thank the University of Tennessee, Knoxville, for a Faculty Leave Award to spend time in the X-ray Crystallography Laboratory at Duke University.

**Supplementary Material Available:**  $^{31}\text{P}\{^1\text{H}\}$  NMR spectra of (A)  $[\text{Rh}_2(\mu\text{-dppm})_2(t\text{-BuNC})_2(\mu\text{-4mpz})(\text{SCN})_2]\text{PF}_6$  and (B)  $[\text{Rh}_2(\mu\text{-dppm})_2(t\text{-BuNC})_2(\mu\text{-pz})(\text{SCN})_2]\text{PF}_6$  (Figure S1), a full table of crystal data (Table S1), and complete lists of bond distances (Table SII), bond angles (Table SIII), hydrogen atom parameters (Table SIV), and anisotropic temperature factor parameters (Table SV) (10 pages); a table of observed and calculated structure amplitudes (Table SVI) (54 pages). Ordering information is given on any current masthead page.

(17) Oro, L. A.; Carmona, D.; Pérez, P. L.; Esteban, M.; Tiripicchio, A.; Tiripicchio-Camellini, M. *J. Chem. Soc., Dalton Trans.* **1985**, 973.

(18) Kang, S.; Albright, T. A.; Wright, T. C.; Jones, R. A. *Organometallics* **1985**, *4*, 666 and references therein.  
 (19) (a) Cowie, M.; Mague, J. T.; Sanger, A. R. *J. Am. Chem. Soc.* **1978**, *100*, 3628. (b) Cowie, M.; Dwight, S. K.; Sanger, A. R. *Inorg. Chim. Acta* **1978**, *31*, L407. (c) Cowie, M.; Dwight, S. K. *Inorg. Chem.* **1979**, *18*, 2700. (d) Cowie, M.; Dwight, S. K. *Inorg. Chem.* **1980**, *19*, 2500. (e) Cowie, M.; Dwight, S. K. *Inorg. Chem.* **1980**, *19*, 2508. (f) Cowie, M.; Dwight, S. K. *J. Organomet. Chem.* **1980**, *198*, C20. (g) Cowie, M.; Dwight, S. K. *J. Organomet. Chem.* **1981**, *214*, 233. (h) Cowie, M.; Southern, T. G. *Inorg. Chem.* **1982**, *21*, 246.  
 (20) Carmona, D.; Oro, L. A.; Pérez, P. L. *J. Chem. Soc., Dalton Trans.* **1989**, 1427.